

Wideband and Compact Impedance-Transforming 90° DC Blocks With Symmetric Coupled Transmission-Line Sections

Hee-Ran Ahn^{ID}, *Senior Member, IEEE*, and Manos M. Tentzeris^{ID}, *Fellow, IEEE*

Abstract—Wideband and compact 90° dc blocks are presented for the impedance-transforming function and designed based on the transmission-zero movement method combined with the pole (root) split method, which is the reason for the wide bandwidth responses, even with being very compact. For a proof-of-concept demonstration, one prototype is tested, and the measured bandwidth with the 10-dB return loss is 0.74–4.05 GHz (331%) with a design frequency of 1 GHz.

Index Terms—Compact 90° dc blocks, impedance-transforming dc blocks, wide bandwidths.

I. INTRODUCTION

A SET of coupled transmission-line sections (CPL) can be used to prevent dc current flow [1]–[18], while permitting RF to flow through. Small and compact capacitors have been used for many applications as the dc blocks. However, as operating frequencies go higher, the lumped element capacitors have disadvantages, one of which is to produce parasitic elements, being difficult to handle. To overcome the problem, distributed dc blocks consisting of arbitrary lengths of CPLs [1]–[18] have been implemented.

For the 90° dc blocks, design formulas were attempted for the symmetric and asymmetric structures in 1980 [2] and 1986 [3], respectively, but seem to be approximate. For this, the improved design formulas were derived in [4] and [5] for the symmetric and asymmetric dc blocks. If its effective electrical lengths of the dc blocks are 90° at the design frequency [2]–[5], real impedance transforming for diverse applications including branch-line couplers is possible.

As the wireless communication systems require substantial reduction in mass and volume, the compactness of the dc blocks has been of high interest. Several works are available for the compact dc blocks [7]–[12]. However, the bandwidths are all low (less than 40 %) [7]–[12] and the sizes are not compact [11]. In this paper, to overcome the conventional problems with small bandwidths, the impedance-transforming wideband and compact 90° dc blocks (WCDCs) will be

treated. The WCDC consists of a CPL, two ports of which are terminated in two identical susceptances and can have wide bandwidths, even with being very compact. The reason for this is they are designed by the combined methods, the pole (root) split (PS) method [4], [5], [19] and the transmission-zero movement (TZM) method that are different from the conventional filter design techniques.

For the verification of the suggested theory, one prototype is designed at 1 GHz and measured 0–5 GHz. The measured bandwidth with the 10-dB return loss is 0.74–4.05 GHz (331%) with a design frequency of 1 GHz, and good agreements between measured and predicted results are achieved, given the fabrication errors.

II. DESIGN METHODS AND COMPACT DC BLOCKS

A. Basic Concept

To enlarge the bandwidths of the passive components, such as impedance transformers, there have been several ways, two of which are the PS and the TZM methods.

1) *Pole Split Method*: In a filter design, to increase the bandwidths, the number of stages (orders) needs to be increased. However, with no increase in the number of stages, the bandwidths can be widened by the PS method. The PS method does not belong to the conventional filter design techniques because the structure itself is not changed, but the responses are changed by the design formulas. One example is the dc blocks with Chebyshev responses [4], [5], and another one is the Butter–Cheby filters [19]. That is, the frequency responses of the 90° dc blocks are changed by the design formulas, but the original structure is kept unchanged.

2) *Transmission-Zero Movement Method*: The TZM method has been used for diverse applications to increase the bandwidths. For example, there are three dc blocks designed at a design frequency of 1 GHz, which are 90°, 60°, and 40° long at 1 GHz. The even- and odd-mode impedances are 103.4 and 23.4 Ω for both termination impedances of 40 Ω . Their frequency responses are plotted in Fig. 1. As can be seen in Fig. 1, the 90° dc block is perfectly matched at 1 GHz, while the two others are not matched at 1 GHz, but perfectly matched at 1.52 and 2.26 GHz, respectively. The bandwidths that can cover the 15-dB return loss in Fig. 1 are red, black, and blue lines with Δ_{40° , Δ_{60° , and Δ_{90° , respectively, and the red line with Δ_{40° is the largest. That is, the bandwidths with the 15-dB return loss are inversely proportional to the

Manuscript received November 20, 2017; revised February 10, 2018; accepted April 24, 2018. Date of publication June 13, 2018; date of current version January 17, 2019. Recommended for publication by Associate Editor T. Wu upon evaluation of reviewers' comments. (*Corresponding author: Hee-Ran Ahn.*)

The authors are with the School of Electrical and Computer Engineering, Georgia Institute of Technology, Atlanta, GA 30332 USA (e-mail: hranahn@gmail.com; etentze@ece.gatech.edu).

Color versions of one or more of the figures in this paper are available online at <http://ieeexplore.ieee.org>.

Digital Object Identifier 10.1109/TCPMT.2018.2838327

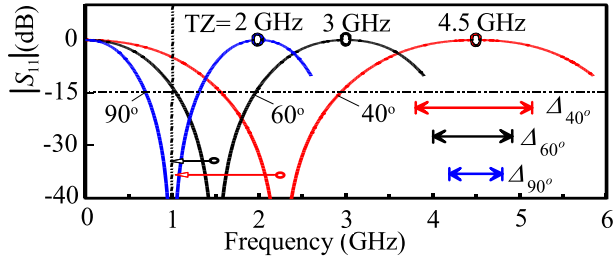


Fig. 1. Frequency responses of $|S_{11}|$ of dc blocks with the electrical lengths of 90° , 60° , and 40° at 1 GHz.

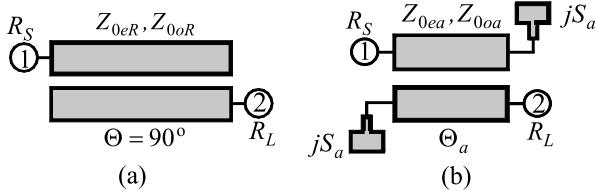


Fig. 2. (a) 90° dc block. (b) WCDC.

electrical lengths of the dc blocks. The reason for this is that the first TZ frequencies of the 90° , 60° , and 40° dc blocks (except 0 GHz) are moved to higher frequency region, such as 2, 3, and 4.5 GHz as shown in Fig. 1. With fixing the TZ frequencies, the matching frequency of the 60° or 40° dc block needs to be shifted to the design frequency of 1 GHz to make the coverage form from around 1 GHz. To move the matching frequency means to build matching circuit using 60° or 40° dc block by adding susceptances so that the resulting circuits can be perfectly matched at 1 GHz and the effective electrical lengths are 90° at 1 GHz. For this, careful matching processes are required.

In this paper, a way that combines the above-mentioned two (PS and TZM) methods will be applied to have the wide bandwidths of the dc blocks. Due to the fundamental reason, the frequency performances of the dc blocks to be treated in this paper are better than those of the conventional filters in terms of bandwidth versus size.

III. COMPACT DC BLOCKS

A 90° dc block terminated in real impedances of R_S and R_L and its WCDC are shown in Fig. 2(a) and (b), respectively, where the impedance parameters of the 90° dc block in Fig. 2(a) [4, eq. (1) with a symmetric case] are

$$\begin{bmatrix} v_1 \\ v_2 \end{bmatrix} = -j \frac{Z_{0eR} - Z_{0oR}}{2} \begin{bmatrix} 0 & 1 \\ 1 & 0 \end{bmatrix} \begin{bmatrix} i_1 \\ i_2 \end{bmatrix} \quad (1)$$

where Z_{0eR} and Z_{0oR} are the even- and odd-mode impedances and the values of Z_{0eR} and Z_{0oR} are determined by the Butterworth response [4].

The WCDC in Fig. 2(b) consists of one CPL with the even- and odd-mode impedances of Z_{0ea} and Z_{0oa} and the electrical length of Θ_a , and two identical susceptances of S_a . The design formulas for the WCDCs will be derived.

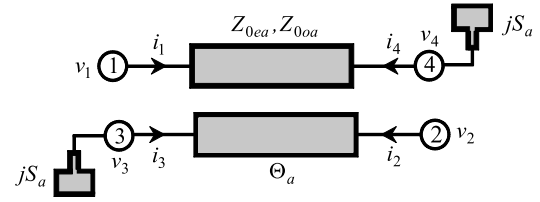


Fig. 3. WCDC with currents and voltages.

A. WCDCs

To design the WCDC in Fig. 2(b), a four-port CPL with Z_{0ea} , Z_{0oa} , and Θ_a should be considered first as shown in Fig. 3, where the port-currents and voltages are indicated. The impedance parameters of the four-port CPL in Fig. 3 [20, eq. (4)] are

$$[\mathbf{Z}] = \begin{bmatrix} Z_{11a} & Z_{12a} & Z_{13a} & Z_{14a} \\ Z_{12a} & Z_{11a} & Z_{14a} & Z_{13a} \\ Z_{13a} & Z_{14a} & Z_{11a} & Z_{12a} \\ Z_{14a} & Z_{13a} & Z_{12a} & Z_{11a} \end{bmatrix} \quad (2)$$

where

$$Z_{11a} = -\frac{j(Z_{0ea} + Z_{0oa})}{2} \cot \Theta_a \quad (2a)$$

$$Z_{12a} = -j \frac{(Z_{0ea} - Z_{0oa})}{2} \csc \Theta_a \quad (2b)$$

$$Z_{13a} = -j \frac{(Z_{0ea} - Z_{0oa})}{2} \cot \Theta_a \quad (2c)$$

$$Z_{14a} = -j \frac{(Z_{0ea} + Z_{0oa})}{2} \csc \Theta_a. \quad (2d)$$

Partitioning the impedance matrix in (2) gives

$$\begin{bmatrix} v_1 \\ v_2 \end{bmatrix} = \mathbf{M}_{11a} \begin{bmatrix} i_1 \\ i_2 \end{bmatrix} + \mathbf{M}_{12a} \begin{bmatrix} i_3 \\ i_4 \end{bmatrix} \quad (3a)$$

$$\begin{bmatrix} v_3 \\ v_4 \end{bmatrix} = \mathbf{M}_{21a} \begin{bmatrix} i_1 \\ i_2 \end{bmatrix} + \mathbf{M}_{22a} \begin{bmatrix} i_3 \\ i_4 \end{bmatrix} \quad (3b)$$

where

$$\mathbf{M}_{11a} = \mathbf{M}_{22a} = \begin{bmatrix} Z_{11a} & Z_{12a} \\ Z_{12a} & Z_{11a} \end{bmatrix} \quad (3c)$$

$$\mathbf{M}_{12a} = \mathbf{M}_{21a} = \begin{bmatrix} Z_{13a} & Z_{14a} \\ Z_{14a} & Z_{13a} \end{bmatrix}. \quad (3d)$$

Terminating at ports ③ and ④ in the identical susceptances of S_a gives the relation as

$$i_3 = -j S_a v_3, \quad i_4 = -j S_a v_4. \quad (4)$$

Substituting the relations in (4) into (3) yields

$$\begin{bmatrix} v_1 \\ v_2 \end{bmatrix} = \mathbf{M}_{11a} \begin{bmatrix} i_1 \\ i_2 \end{bmatrix} - j S_a \mathbf{M}_{12a} \begin{bmatrix} v_3 \\ v_4 \end{bmatrix} \quad (5a)$$

$$\begin{bmatrix} v_3 \\ v_4 \end{bmatrix} = \mathbf{M}_{21a} \begin{bmatrix} i_1 \\ i_2 \end{bmatrix} - j S_a \mathbf{M}_{22a} \begin{bmatrix} v_3 \\ v_4 \end{bmatrix}. \quad (5b)$$

Equation (5b) is simplified as

$$(U + j S_a \mathbf{M}_{22a}) \begin{bmatrix} v_3 \\ v_4 \end{bmatrix} = \mathbf{M}_{21a} \begin{bmatrix} i_1 \\ i_2 \end{bmatrix} \quad (6)$$

where

$$U = \begin{bmatrix} 1 & 0 \\ 0 & 1 \end{bmatrix}.$$

From (4)–(6), the impedance matrix between ports ① and ② can be obtained as (7)

$$\begin{bmatrix} v_1 \\ v_2 \end{bmatrix} = \mathbf{F}_a \begin{bmatrix} i_1 \\ i_2 \end{bmatrix} = \begin{bmatrix} F_{11a} & F_{12a} \\ F_{21a} & F_{22a} \end{bmatrix} \begin{bmatrix} i_1 \\ i_2 \end{bmatrix} \quad (7)$$

where

$$\mathbf{F}_a = \mathbf{M}_{11a} - jS_a \mathbf{M}_{12a} (\mathbf{U} + jS_a \mathbf{M}_{22a})^{-1} \mathbf{M}_{21a} \quad (7a)$$

leading to

$$F_{11a} = F_{22a} = Z_{11a} - \frac{jS_a}{D_a} \{ (1 + jS_a Z_{11a})(Z_{13a}^2 + Z_{14a}^2) - j2S_a Z_{12a} Z_{13a} Z_{14a} \} \quad (7b)$$

$$F_{12a} = F_{21a} = Z_{12a} - \frac{jS_a}{D_a} \{ 2(1 + jS_a Z_{11a})Z_{13a} Z_{14a} - jS_a Z_{12a} (Z_{13a}^2 + Z_{14a}^2) \} \quad (7c)$$

$$D_a = (1 + jS_a Z_{11a})^2 - (jS_a Z_{12a})^2.$$

The susceptance of S_a can be realized with an open stub as

$$S_a = \sqrt{Y_{0eR} Y_{0oR}} \tan \Theta_{Ta} = Y_{Ta} \tan \Theta_{Ta} \quad (8)$$

where

$$Y_{0eR} = Z_{0eR}^{-1} \quad \text{and} \quad Y_{0oR} = Z_{0oR}^{-1}.$$

The matrix of \mathbf{F}_a (7a) should be equal to those of the 90° dc block in (1), from which the design formulas for Θ_a , Z_{0ea} , and Z_{0oa} are obtained as follows:

$$\cos \Theta_a = \frac{\cos \Theta_{Ta} \{ 4S_a^2 + \tan^2 \Theta_{Ta} (Y_{0eR} - Y_{0oR})^2 \}}{2S_a (Y_{0eR} + Y_{0oR})} \quad (9a)$$

$$Y_{0ea} = Z_{0ea}^{-1} = \frac{2S_a^2 \csc \Theta_{Ta}}{\csc \Theta_a} \psi_e \quad (9b)$$

$$Y_{0oa} = Z_{0oa}^{-1} = \frac{2S_a^2 \csc \Theta_{Ta}}{\csc \Theta_a} \psi_o \quad (9c)$$

where $\Theta_{Ta} \neq 0$ and

$$\psi_e = \frac{(\cot \Theta_{Ta} + \csc \Theta_{Ta}) Y_{0eR} + (\cot \Theta_{Ta} - \csc \Theta_{Ta}) Y_{0oR}}{(2S_a \cot \Theta_{Ta})^2 - \tan^2 \Theta_{Ta} (Y_{0eR} - Y_{0oR})^2} \quad (9d)$$

$$\psi_o = \frac{(\cot \Theta_{Ta} - \csc \Theta_{Ta}) Y_{0eR} + (\cot \Theta_{Ta} + \csc \Theta_{Ta}) Y_{0oR}}{(2S_a \cot \Theta_{Ta})^2 - \tan^2 \Theta_{Ta} (Y_{0eR} - Y_{0oR})^2} \quad (9e)$$

Z_{0eR} and Z_{0oR} of the 90° dc block are determined by Butterworth response in [4, eqs. (14) and (24) with $R_{ip} = 0$] and expressed as

$$Z_{0eR} = \sqrt{R_S R_L} \frac{1 + C_T}{C_T} \quad (10a)$$

$$Z_{0oR} = \sqrt{R_S R_L} \frac{1 - C_T}{C_T} \quad (10b)$$

where C_T is a coupling coefficient.

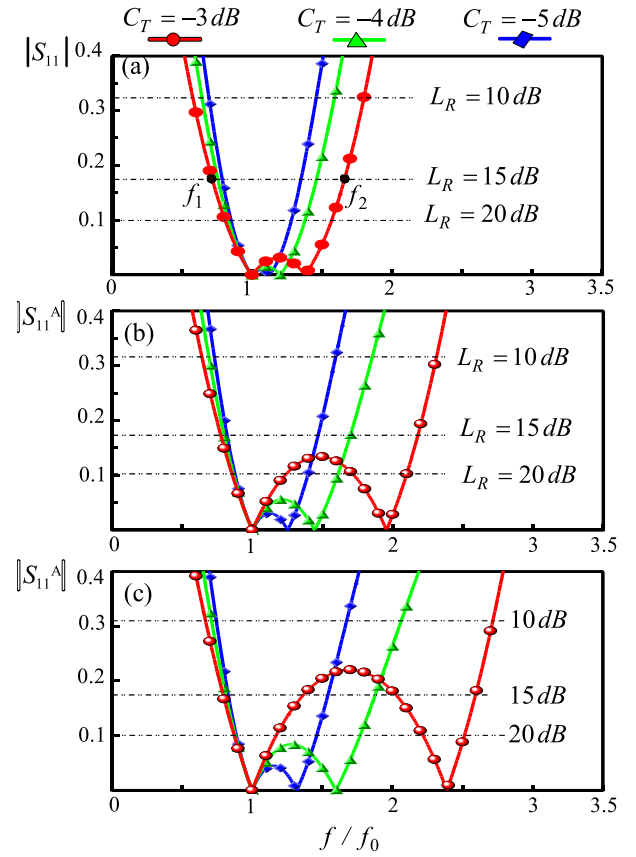


Fig. 4. Frequency responses of $|S_{11}|$. (a) $\Theta_{Ta} = 10^\circ$. (b) $\Theta_{Ta} = 20^\circ$. (c) $\Theta_{Ta} = 25^\circ$.

Scattering parameter of S_{11} can be formulated [21] as

$$S_{11} \left(\frac{f}{f_0} \right) = \frac{\left\{ F_{11a} \left(\frac{f}{f_0} \right) - R_S \right\} \left\{ F_{11a} \left(\frac{f}{f_0} \right) + R_L \right\} - F_{12a} \left(\frac{f}{f_0} \right)^2}{\left\{ F_{11a} \left(\frac{f}{f_0} \right) + R_S \right\} \left\{ F_{11a} \left(\frac{f}{f_0} \right) + R_L \right\} - F_{12a} \left(\frac{f}{f_0} \right)^2} \quad (11)$$

where f and f_0 are operating and design frequencies.

$R_S = R_L = 40 \Omega$, $C_T = -3, -4$, and -5 dB being substituted into (10a) and (10b), the even- and odd-mode impedances of Z_{0eR} and Z_{0oR} of the 90° dc blocks are calculated for the Butterworth responses as $(Z_{0eR}, Z_{0oR}) = (96.5 \Omega, 16.5 \Omega)$, $(103.4 \Omega, 23.4 \Omega)$, and $(111.1 \Omega, 31.1 \Omega)$, respectively. With the values of (Z_{0eR}, Z_{0oR}) , varying $\Theta_{Ta} = 10^\circ, 20^\circ$, and 25° in (8), the even- and odd-mode impedances Z_{0ea} and Z_{0oa} along with the electrical lengths Θ_a of the WCDCs can be calculated based on (9).

The scattering parameters of $|S_{11}|$ with the calculated values of Z_{0ea} , Z_{0oa} , and Θ_a can be calculated based on (11), or can be obtained by a circuit simulator like ADS, as shown in Fig. 4, where those with $\Theta_{Ta} = 10^\circ, 20^\circ$, and 25° are displayed in Fig. 4(a)–(c), respectively, where f_0 and f are the design and operating frequencies, and the return loss values of L_R are indicated. For $\Theta_{Ta} = 10^\circ$ in Fig. 4(a), the response of $|S_{11}|$ with $C_T = -3$ dB intersects a line indicating $L_R = 15$ dB at

TABLE I
 BANDWIDTHS DEPENDING ON L_R AND C_T

Θ_{Ta}	$C_T = -3$ dB		$C_T = -4$ dB	
	10°	20°	10°	20°
10 dB	120 %	167 %	93 %	117 %
15 dB	93 %	141 %	70 %	91 %
20 dB	76 %	123 %	53 %	73 %

 TABLE II
 DESIGN PARAMETERS FOR Z_{0ea} , Z_{0oa} , AND Θ_a WITH
 $Z_{0eR} = 103.40 \Omega$ AND $Z_{0oR} = 23.40 \Omega$

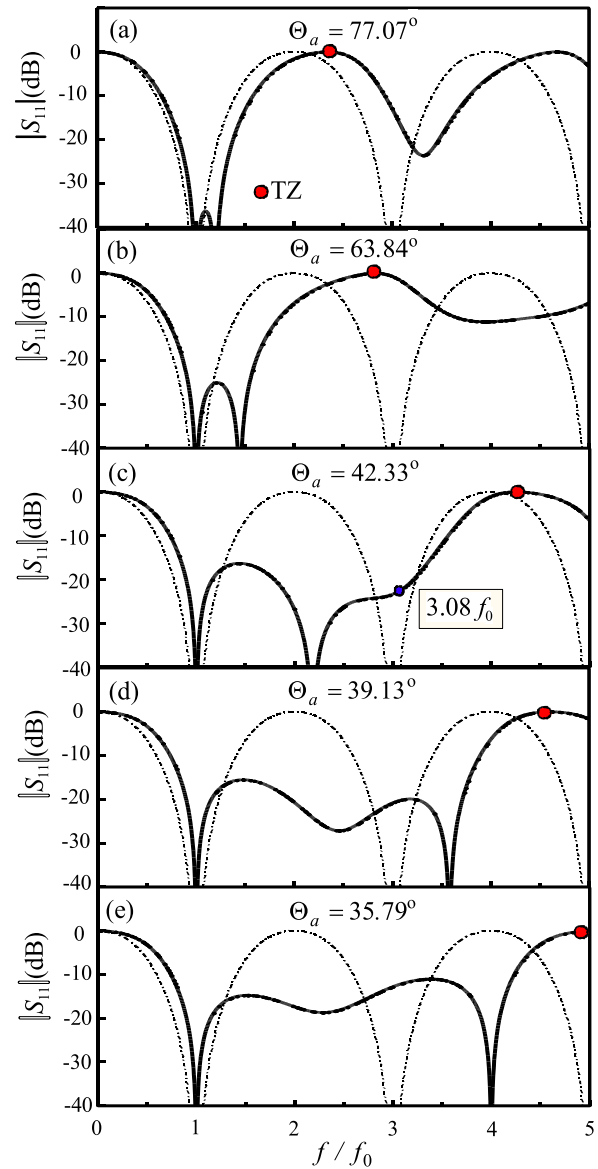
$S_a^{-1}(\Omega)$	$Z_{0ea}(\Omega)$	$Z_{0oa}(\Omega)$	$\Theta_a(^\circ)$
278.93 (10°)	105.1	23.02	77.07
135.13 (20°)	110.93	21.81	63.84
70.24 (35°)	136.53	17.72	42.33
65.27 (37°)	143.61	16.84	39.13
60.74 (39°)	152.64	15.85	35.79

two points f_1 and f_2 , and the bandwidth with $L_R = 15$ dB is defined as $(f_2 - f_1)/f_0$. In this way, the bandwidths are calculated in Table I, where the calculation values find that with longer lengths of Θ_{Ta} (or shorter lengths of Θ_a) and with higher values of C_T , wider bandwidths can be obtained in some degree.

When the value of S_a^{-1} is given as 278.9 Ω in Figs. 2(b) and 3, substituting the values of S_a^{-1} , $Z_{0eR} = 103.4 \Omega$, and $Z_{0oR} = 23.4 \Omega$ for $C_T = -4$ dB into (9) gives the even- and odd-mode impedances of $Z_{0ea} = 105.1 \Omega$ and $Z_{0oa} = 23.02 \Omega$ and the electrical length of $\Theta_a = 77.07^\circ$ of the WCDCs. In this way, the design parameters can be obtained in Table II, where $Z_{Ta} = 49.18 \Omega$ can be calculated from (8) and the values in parentheses are for Θ_{Ta} to have the required values of S_a^{-1} .

With the electrical length of Θ_a shorter, since the coupling lengths become shorter, the values of Z_{0ea} increase and those of Z_{0oa} decrease to make up for the lacking coupling generated by reducing the coupling lengths. Based on the design parameters in Table II, the WCDCs were simulated with ADS and the frequency responses of $|S_{11}|$ are plotted in the range of $(0-5) f_0$ in Fig. 5, where the dotted lines are those with the original 90° dc block in Fig. 2(a), and solid lines are those of the WCDCs in Fig. 2(b). Each susceptance of S_a was realized with an open stub having the uniform characteristic impedance of 49.18Ω from (8). In this case, $R_S = R_L = 40 \Omega$.

The maximum number of roots for the solutions to $S_{11}(f/f_0) = 0$ (11) is four in a range of $0 - (180^\circ/\Theta_a)f_0$, and the real roots are called poles. All the WCDCs in Fig. 5 are perfectly matched at f_0 , and the bandwidth with $L_R = 10$ dB of the 90° dc block is about $0.6-1.41 f_0$ (81%). On the other hand, the 10-dB bandwidth with $\Theta_a = 77.07^\circ$ in Fig. 5(a) is $0.65-1.585 f_0$ (93.5%). That with $\Theta_a = 64.84^\circ$ in Fig. 5(b) is $0.69-1.86 f_0$ (117%). Those with $\Theta_a = 42.33^\circ$, 39.13° , and 35.79° in Fig. 5(c)-(e) are $0.74-3.57 f_0$ (283%),


 Fig. 5. Frequency responses of $|S_{11}|$ with $C_T = -4$ dB. (a) $\Theta_a = 77.07^\circ$. (b) $\Theta_a = 63.84^\circ$. (c) $\Theta_a = 42.33^\circ$. (d) $\Theta_a = 39.13^\circ$. (e) $\Theta_a = 35.79^\circ$.

$0.74-3.9 f_0$ (316%), and $0.74-4.24 f_0$ (350%), respectively, and inversely proportional to the electrical length of Θ_a .

When $\Theta_a = 90^\circ$, the WCDC becomes the original 90° dc block and two poles for the perfect matching are overlapped at f_0 . When Θ_a becomes shorter than 90° , any value of S_a is needed for the perfect matching at f_0 as explained in Fig. 1 and the overlapped two poles at f_0 start to be split, or PS method. For $\Theta_a = 77.07^\circ$ in Fig. 5(a), one pole is at f_0 , and another is at $1.2 f_0$. For $\Theta_a = 42.33^\circ$ in Fig. 5(c), two poles exist at f_0 and $2.18 f_0$, and two complex roots exist around $3.08 f_0$ and can be developed into real roots with slight changes. As the electrical lengths of Θ_a become shorter, the two roots (poles) close to the TZs $\{0 \text{ GHz and } (180^\circ/\Theta_a)f_0\}$ are located further away, which is the main reason for enlarging the bandwidths. That is, the TZs are moved further as the red dots are indicated in Fig. 5, which is the TZM method.

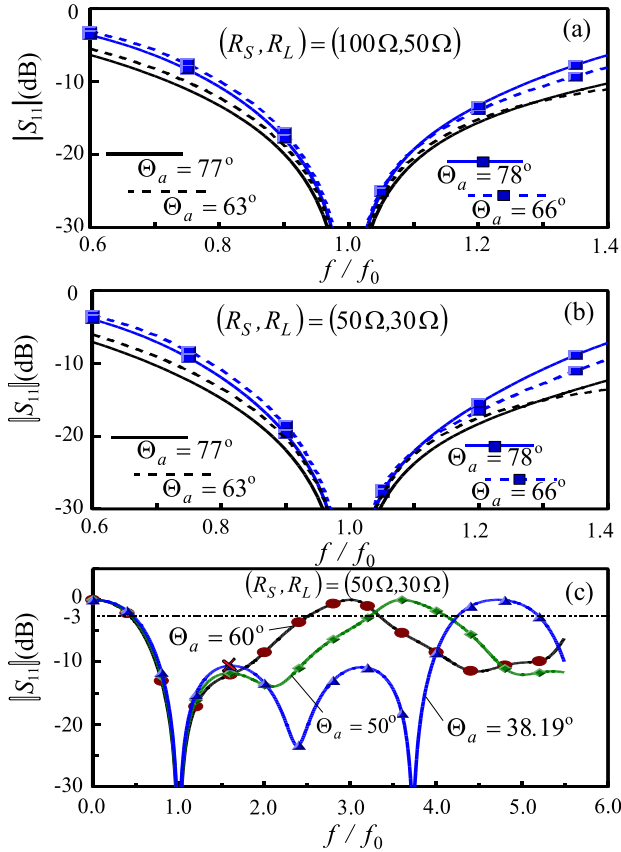


Fig. 6. Frequency responses of the impedance-transforming WCDCs. (a) $(R_S, R_L) = (100 \Omega, 50 \Omega)$. (b) $(R_S, R_L) = (50 \Omega, 30 \Omega)$ for Θ_a greater than 63° . (c) $(R_S, R_L) = (50 \Omega, 30 \Omega)$ for Θ_a less than 60° .

B. Impedance-Transforming WCDCs

Since the effective electrical length of the WCDCs is 90° at f_0 , any impedance transforming is possible and there is no limitation around design frequency. The design parameters of the two cases for $(R_S, R_L) = (100 \Omega, 50 \Omega)$ and $(50 \Omega, 30 \Omega)$ are listed for $C_T = -4$ dB and $C_T = -6$ dB in Table III based on which the frequency responses of $|S_{11}|$ are plotted in Fig. 6, where those for $(R_S, R_L) = (100 \Omega, 50 \Omega)$ are plotted in Fig. 6(a), while those for $(R_S, R_L) = (50 \Omega, 30 \Omega)$ are in Fig. 6(b) and (c), where the responses for Θ_a greater than 63° are in Fig. 6(b), while those for Θ_a less than 60° are in Fig. 6(c).

As can be seen in Fig. 6(a) and (b), all are perfectly matched at f_0 , regardless of the termination impedance values, and the bandwidths with $\Theta_a = 77^\circ$ and 63° (black solid and dotted lines) for $C_T = -4$ dB (see Table III) are slightly wider than those with $\Theta_a = 78^\circ$ and 66° (blue solid and dotted lines with symbols) for $C_T = -6$ dB.

For $(R_S, R_L) = (50 \Omega, 30 \Omega)$ in Fig. 6(c), the bandwidths become wider with smaller lengths of Θ_a , but due to the lowest return loss value for $\Theta_a = 38.19^\circ$ expressed as a red cross between two poles at 1 GHz and around 3.5 GHz, the bandwidths with L_R greater than 10 dB are restricted somehow, which is similar to quarter-wave impedance transformers with higher impedance transformation ratios.

TABLE III
DESIGN PARAMETERS FOR IMPEDANCE TRANSFORMING

C_T (dB)	Θ_{Ta} ($^\circ$)	Z_{0ea} (Ω)	Z_{0oa} (Ω)	Θ_a ($^\circ$)	Z_{Ta} (Ω)
$(R_S, R_L) = (100 \Omega, 50 \Omega)$					
-4	10	185.79	40.69	77.07	86.95
-4	20	196.11	38.55	63.84	86.95
-6	10	214.0	69.65	78.42	122.09
-6	20	221.31	67.35	66.72	122.09
$(R_S, R_L) = (50 \Omega, 30 \Omega)$					
-4	10	101.76	22.29	77.07	47.62
-4	20	107.41	21.11	63.84	47.62
-6	10	117.22	38.15	78.42	66.87
-6	20	121.22	36.89	66.72	66.87
-4	22.82	110.0	20.61	60.0	47.62
-4	29.9	120.0	18.9	50.0	47.62
-4	37.52	141.3	16.1	38.19	47.62

IV. VERIFICATION WITH MEASUREMENTS

For the verification of the suggested theory, one prototype was fabricated on a substrate (RO3003, $\epsilon_r = 3$ and $H = 0.75$ mm).

A. Measurements

For the measurements, the electrical length of Θ_a in Table II is chosen as 39.13° , where the corresponding values are $Z_{0ea} = 143.61 \Omega$, $Z_{0oa} = 16.84 \Omega$, and $S_a^{-1} = 65.27 \Omega$. To realize S_a , two transmission-line sections connected in cascade are employed, one of which is high-impedance line, and another of which is low-impedance line. The characteristic impedances of the high-low-impedance line are 140 and 35Ω , and the electrical lengths are 6.0° and 22° at 1 GHz with the form in [22, Fig. 13(b)]. One side of the low-impedance line is open-circuited, and another side is connected to the high-impedance line, which is located between the low-impedance line and the CPL.

Since the required even- and odd-mode impedances have a tight coupling higher than -3 dB, 2-D microstrip format may be impossible, and strip lines, microstrip coupled lines with defected ground structure (DGS) [10], multiconductor lines [23], [24], and vertically installed planar (VIP) [25]–[27] are good candidates for such a tight coupling. However, since the strip lines use a flat strip of metal that is sandwiched between two parallel ground planes, the fabrication process may be complicated. The possibility of such tight coupling is demonstrated with DGS in [10], but the exact design formulas are not established. Such a tight coupling may also be feasible with multiconductor lines, but the resulting even-mode impedance becomes too high to fabricate on the given substrate. Thus, in this paper, the tight coupling will be fabricated with the VIP using the 3-D structure as shown in [25, Fig. 18(b)].

To realize both Z_{0ea} and Z_{0oa} , first consider the 2-D structure in [25, Fig. 18(a)] that can have $Z'_{0ea} = 143.61 \Omega$ and $Z'_{0oa} = 67.45 \Omega$ in [25, eq.(21)], whose physical

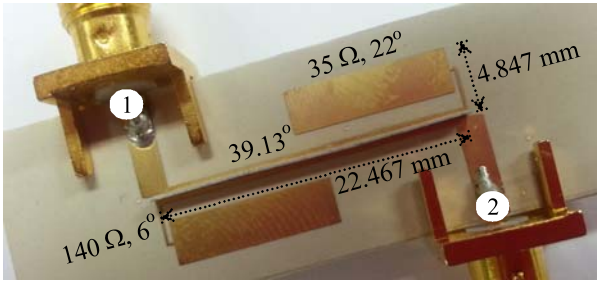
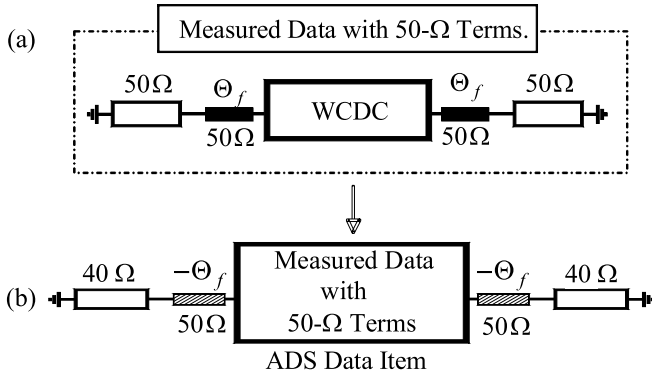


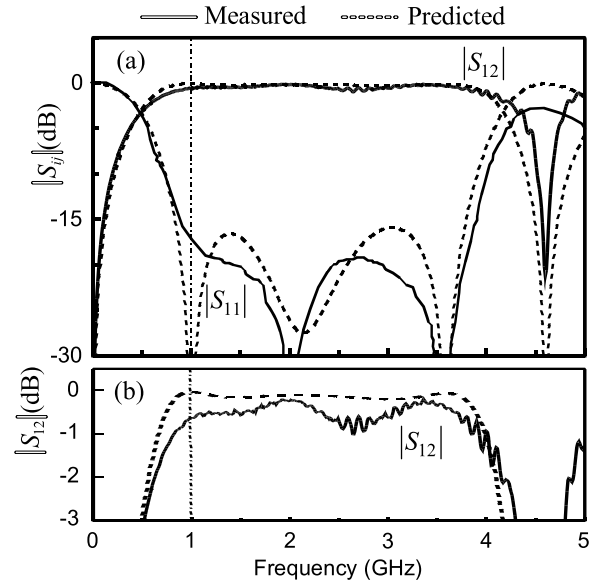
Fig. 7. Fabricated WCDC.


 Fig. 8. Measured data transformation. (a) 50- Ω termination impedances. (b) 40- Ω termination impedance.

dimensions are width $w_c = 0.39$ mm and gap $g \approx 0.25$ mm (10 mil) in [25, Fig. 18(a)]. For the case with $Z_{0oa} = 16.84 \Omega$ and $Z'_{0oa} = 67.45 \Omega$, which are the same as Z_{0o} and Z'_{0o} , respectively, in [25, eq. (23)], the capacitance of $2C_v$ in [25, Fig. 18(b)] and [28] is calculated as $(\epsilon_{\text{eff}}\mu)^{1/2}/22.45$, which implies that the impedance due to the capacitance of $2C_v$ is 22.45Ω . The width w_v in [25, Fig. 18(b)] for the characteristic impedance is easily obtained in the way shown in [25, Fig. 19] by a 3-D commercial simulator like HFSS as $w_v = 0.93$ mm. The fabricated WCDC is shown in Fig. 7.

Since the WCDC is terminated in 40Ω , the 50-measurement system may not be suitable without impedance transformers. One of ways for the 50- Ω measurements is as follows. Letting the targeting circuit for the measurements be WCDC in Fig. 8(a), the characteristics of the WCDC are not changed by the termination impedances. That is, impedance, admittance, and ABCD parameters of the WCDC are not changed by the termination impedances, but only scattering parameters are changed by the termination impedances. The WCDC is measured in the form in Fig. 8(a), where the characteristic impedance and the electrical length of the feeding lines are assumed to be 50Ω and Θ_f , respectively. After measuring the scattering parameter of the WCDC with the 50- Ω termination impedances, save the measured data in the ADS data item as shown in Fig. 8(b).

Since the saved data contain the feeding lines, the effect should be removed by adding two transmission-line sections with the characteristic impedance of 50Ω but the electrical length of $-\Theta_f$. For the measured data, terminate it in the desired termination impedance of 40Ω as shown in Fig. 8(b) and simulate it once more. Then, the converted


 Fig. 9. Measured and predicted frequency responses of WCDC. (a) $|S_{12}|$ and $|S_{11}|$. (b) Close view of $|S_{12}|$.

data are obtained, and they can be the measured data with 40- Ω -termination impedances. The measured frequency responses of $|S_{11}|$ and $|S_{12}|$ are in Fig. 9(a), while the close view of $|S_{12}|$ is in Fig. 9(b). The measured bandwidth with 10-dB return loss in Fig. 11(a) is 0.74–4.05 GHz (331%) with the design frequency of 1 GHz. At the design frequency of 1 GHz, the measured $|S_{12}|$ is about -0.634 dB.

B. Comparisons With Conventional Works

The prototype is compared with the conventional ones [2], [4], [7], [8], [10], [11], and compared results are listed in Table IV where the “total TL.” means total CPLs, “Arb. Term.” indicates arbitrary termination impedances, “o” or “x” is possibility or impossibility, “Passband” is a frequency region where the return loss is greater than 10 dB, and f_0 is a design frequency. The measured prototype is only 39.13° long, but the bandwidth is 331%, and the impedance transforming is possible because the effective electrical lengths are 90° as demonstrated in Fig. 6. The CPLs of the dc blocks in [7], [8], [10], and [11] are 45° , 67.12° , 38.19° , and 95° long, respectively, and the bandwidths are 40%, 20%, 37%, and 32.5%, respectively, as written in Table IV. The insertion loss of the measured prototype is 0.63 dB at 1 GHz, while the others at the design center frequencies are 0.6–0.8 dB [2], 0.19 dB [4], 1.0 dB [7], 0.5 dB [8], and 2 dB [11].

The dc blocks in Table IV are designed at f_0 , and their frequency responses except for the prototype in this paper are about symmetric with respect to f_0 . Therefore, the design frequency is the same as the center frequency. On the other hand, the prototype is designed at 1 GHz, but the frequency responses are not symmetric with respect to 1 GHz. Thus, the design frequency is not located at the center of the passband, which is the fundamental reason to differentiate this paper from the conventional designs. Furthermore, the

TABLE IV
COMPARISON OF THIS PAPER WITH CONVENTIONAL ONES

	Total TL.	Arb. Term.	Pass-band / f_0
This work	39.13°	o	0.74 - 4.05 = 331 %
[2]	90°	x	0.68 - 1.33 = 65%
[4]	90°	o	0.68 - 1.33 = 65%
[7]	45°	x	0.80 - 1.20 = 40%
[8]	67.25°	x	0.90 - 1.10 = 20%
[10]	38.19°	o	0.80 - 1.17 = 37%
[11]	95°	x	0.85-1.175=32.5%

passband region of the prototype is much wider than the conventional works even with the compacter size.

V. CONCLUSION

In this paper, the impedance-transforming WDCs are presented. The WDCs can be much shorter than 90° long, but the bandwidths can be much wider than those of the convention ones as demonstrated in Table IV. The WDCs each consist of a CPL with two ports terminated in two identical susceptances in a diagonal direction, and the bandwidths increase gradually as the CPL becomes shorter in a certain range. The reason for the wide bandwidths is that the WDCs are designed using the combined PS and TZM methods.

Since the presented dc blocks are compact and can have wide bandwidths with additional impedance-transforming functions, many applications can be expected in diverse applications.

REFERENCES

- [1] D. Lacombe and J. Cohen, "Octave-band microstrip DC blocks," *IEEE Trans. Microw. Theory Techn.*, vol. MTT-20, no. 8, pp. 555–556, Aug. 1972.
- [2] D. Kajfez and B. S. Vidula, "Design equations for symmetric microstrip DC blocks," *IEEE Trans. Microw. Theory Techn.*, vol. MTT-28, no. 9, pp. 974–981, Sep. 1980.
- [3] A. Podcameni, "Symmetrical and asymmetrical edge-coupled-line impedance transformers with a prescribed insertion loss design," *IEEE Trans. Microw. Theory Techn.*, vol. MTT-34, no. 1, pp. 1–6, Jan. 1986.
- [4] H.-R. Ahn and T. Itoh, "Impedance-transforming symmetric and asymmetric DC blocks," *IEEE Trans. Microw. Theory Techn.*, vol. 58, no. 9, pp. 2463–2474, Sep. 2010.
- [5] H.-R. Ahn and T. Itoh, "Corrections to 'impedance-transforming symmetric and asymmetric DC blocks,'" *IEEE Trans. Microw. Theory Techn.*, vol. 59, no. 1, p. 207, Jan. 2011.
- [6] S. R. Borgaonkar and S. N. Rao, "Analysis and design of DC blocks," *Electron. Lett.*, vol. 17, no. 2, pp. 101–103, Jan. 1981.
- [7] S.-H. Choi, J.-Y. Lee, K.-B. Lee, and D.-H. Shin, "Design of miniaturized symmetric microstrip DC block," in *Proc. APMC*, Dec. 2007, pp. 1–4.
- [8] B. Strassner and K. Chang, "New wide-band DC-block cymbal bandpass filter," *IEEE Trans. Microw. Theory Techn.*, vol. 50, no. 5, pp. 1431–1432, May 2002.
- [9] S. Lee and Y. Lee, "Generalized miniaturization method for coupled-line bandpass filters by reactive loading," *IEEE Trans. Microw. Theory Techn.*, vol. 58, no. 9, pp. 2383–2391, Sep. 2010.
- [10] B. Kim, S. Nam, H.-R. Ahn, and J.-H. Song, "Design of wideband coupled line DC block with compact size," *IEICE Trans. Electron.*, vol. E97.C, pp. 915–917, Sep. 2014.
- [11] W. Zhao, Y. Zhang, M. Zhan, L. Li, S. Liu, and R. Xu, "Compact broadband DC-block filter," in *Proc. IEEE Int. Conf. Commun. Problem-Solving*, Dec. 2014, pp. 439–441.
- [12] Y. Wu, Y. Liu, S. Li, and C. Yu, "New coupled-line dual-band DC-block transformer for arbitrary complex frequency-dependent load impedance," *Microw. Opt. Technol. Lett.*, vol. 54, pp. 139–142, Jan. 2012.
- [13] C. E. Free and C. S. Aitchison, "Excess phase in microstrip DC blocks," *Electron. Lett.*, vol. 20, no. 21, pp. 892–893, Oct. 1984.
- [14] V. K. Tripathi, Y. K. Chin, and H. Lee, "Interdigital multiple coupled microstrip DC blocks," in *Proc. 12th Eur. Microw. Conf.*, Sep. 1982, pp. 632–636.
- [15] C. Y. Ho, "Analysis of DC blocks using coupled lines," *IEEE Trans. Microw. Theory Techn.*, vol. 23, no. 9, pp. 773–774, Sep. 1975.
- [16] S. Uysal, M. S. Leong, and P. S. Kooi, "Experimental determination of open-end length extension in coplanar waveguide coupled line DC blocks with finite ground planes," in *Proc. APMC*, Dec. 1997, pp. 977–979.
- [17] C. Friesicke, B. Rohrdantz, A. Stark, and A. F. Jacob, "A vertical interconnect with DC-block using a low-cost technology at mm-wave frequencies," in *Proc. APMC*, Nov. 2014, pp. 277–279.
- [18] T. E. Koscica, "Microstrip quarter-wave high voltage DC block," *IEEE Trans. Microw. Theory Techn.*, vol. 41, no. 1, pp. 162–164, Jan. 1993.
- [19] H.-R. Ahn and S. Nam, "Design method for Butter–Cheby bandpass filters with even number of resonators," *IEEE Trans. Microw. Theory Techn.*, vol. 60, no. 6, pp. 1549–1559, Jun. 2012.
- [20] G. I. Zysman and A. K. Johnson, "Coupled transmission line networks in an inhomogeneous dielectric medium," *IEEE Trans. Microw. Theory Techn.*, vol. MTT-17, no. 10, pp. 753–759, Oct. 1969.
- [21] H.-R. Ahn, *Asymmetric Passive Components in Microwave Integrated Circuits*. Hoboken, NJ, USA: Wiley, 2006, ch. 2.
- [22] H.-R. Ahn and S. Nam, "Compact microstrip 3-dB coupled-line ring and branch-line hybrids with new symmetric equivalent circuits," *IEEE Trans. Microw. Theory Techn.*, vol. 61, no. 3, pp. 1067–1078, Mar. 2013.
- [23] W. P. Ou, "Design equations for an interdigitated directional coupler," *IEEE Trans. Microw. Theory Techn.*, vol. MTT-23, no. 2, pp. 253–255, Feb. 1975.
- [24] A. Presser, "Interdigitated microstrip coupler design," *IEEE Trans. Microw. Theory Techn.*, vol. MTT-26, no. 10, pp. 801–805, Oct. 1978.
- [25] H.-R. Ahn and M. M. Tentzeris, "Novel generic asymmetric and symmetric equivalent circuits of 90° coupled transmission-line sections applicable to marchand baluns," *IEEE Trans. Microw. Theory Techn.*, vol. 65, no. 3, pp. 746–760, Mar. 2017.
- [26] Y. Konishi, I. Awai, Y. Fukuoka, and M. Nakajima, "A directional coupler of a vertically installed planar circuit structure," *IEEE Trans. Microw. Theory Techn.*, vol. 36, no. 6, pp. 1057–1063, Jun. 1988.
- [27] H. R. Ahn and B. Kim, "Small wideband coupled-line ring hybrids with no restriction on coupling power," *IEEE Trans. Microw. Theory Techn.*, vol. 57, no. 7, pp. 1806–1817, Jul. 2009.
- [28] D. M. Pozar, *Microwave Engineering*. Hoboken, NJ, USA: Wiley, 2011, pp. 384–401.



Hee-Ran Ahn (S'90–M'95–SM'99) received the B.S., M.S., and Ph.D. degrees in electronic engineering from Sogang University, Seoul, South Korea.

From 1996 to 2002, she was with the Department of Electrical Engineering, University of Duisburg-Essen, Duisburg, Germany, where she was involved in habilitation dealing with asymmetric passive components in microwave circuits. From 2003 to 2005, she was with the Department of Electrical Engineering and Computer Science, Korea Advanced Institute of Science and Technology, Daejeon, South Korea. From 2005 to 2009, she was with the Department of Electronics and Electrical Engineering, Pohang University of Science and Technology, Pohang, South Korea. From 2009 to 2010, she was with the Department of Electrical Engineering, University of California at Los Angeles, Los Angeles, CA, USA. From 2011 to 2014, she was with the School of Electrical Engineering and Computer Science, Seoul National University, Seoul Korea. Since 2015, she has been with the School of Electrical and Computer Engineering, Georgia Institute of Technology, Atlanta, GA, USA, as a Visiting Scholar. She authored a book *Asymmetric Passive Component in Microwave Integrated Circuits* (Wiley, 2006). Her current research interests include high-frequency and microwave circuit designs and biomedical applications using microwave theory and techniques.



Manos M. Tentzeris (M'98–SM'03–F'10) received the Diploma degree (*magna cum laude*) in electrical and computer engineering from the National Technical University of Athens, Athens, Greece, and the M.S. and Ph.D. degrees in electrical engineering and computer science from the University of Michigan, Ann Arbor, MI, USA.

He was a Visiting Professor with the Technical University of Munich, Munich, Germany, in 2002; the Georgia Tech Research Institute, Athlone, Ireland, in 2009; and LAAS-CNRS, Toulouse, France, in 2010. He has served as the Head of the Electromagnetics Technical Interest Group, School of Electrical and Computer Engineering, Georgia Institute of Technology, Atlanta, GA, USA; the Associate Director for RFID/Sensors Research, Georgia Electronic Design Center, Atlanta; and the Associate Director for RF Research and the RF Alliance Leader Georgia Tech NSF-Packaging Research Center, Atlanta. He is currently the Ken Byers Professor in flexible electronics with the School of Electrical and Computer Engineering, Georgia Institute of Technology, where he is also the Head of the Adaptive Techniques in Hybrid Electromagnetic Numerical Applications Group (20 researchers). He has authored over 620 papers in refereed journals and conference proceedings, five books, and 25 book chapters. He has helped develop academic programs in 3-D/inkjet-printed RF electronics and modules, flexible electronics, origami and morphing electromagnetics, highly integrated/multilayer packaging for RF and wireless applications using ceramic and organic flexible materials, paper-based RFIDs and sensors, wireless sensors and biosensors, wearable electronics, green electronics, energy harvesting and wireless power transfer, nanotechnology applications in RF, microwave MEMS, and SOP-integrated (ultrawideband, multiband, millimeter-wave, and conformal) antennas.

Dr. Tentzeris is a member of the URSI-Commission D, the MTT-15 Committee, and the Technical Chamber of Greece, an Associate Member of EuMA, and a fellow of the Electromagnetic Academy. He was a recipient/co-recipient of the 1997 Best Paper Award at the International Hybrid Microelectronics

and Packaging Society, the 2000 NSF CAREER Award, the 2001 ACES Conference Best Paper Award, the 2002 International Conference on Microwave and Millimeter-Wave Technology Best Paper Award, Beijing, China, the 2002 Georgia Tech-Electrical and Computer Engineering Outstanding Junior Faculty Award, the 2003 NASA Godfrey "Art" Anzic Collaborative Distinguished Publication Award, the 2003 IBC International Educator of the Year Award, the 2003 IEEE CPMT Outstanding Young Engineer Award, the 2004 IEEE TRANSACTIONS ON ADVANCED PACKAGING Commendable Paper Award, the 2006 IEEE MTT Outstanding Young Engineer Award, the 2006 Asia-Pacific Microwave Conference Award, the 2007 IEEE APS Symposium Best Student Paper Award, the 2007 IEEE IMS Third Best Student Paper Award, the ISAP 2007 Poster Presentation Award, the 2009 IEEE TRANSACTIONS ON COMPONENTS AND PACKAGING TECHNOLOGIES Best Paper Award, the 2009 E. T. S. Walton Award from the Irish Science Foundation, the 2010 Georgia Tech Senior Faculty Outstanding Undergraduate Research Mentor Award, the 2010 IEEE Antennas and Propagation Society Piergiorgio L. E. Uslenghi Letters Prize Paper Award, the 2011 International Workshop on Structural Health Monitoring Best Student Paper Award, the 2012 FiDiPro Award in Finland, the iCMG Architecture Award of Excellence, the *IET Microwaves, Antennas and Propagation* Premium Award in 2013 and 2015, respectively, the 2014 Georgia Tech Electrical and Computer Engineering Distinguished Faculty Achievement Award, and the 2014 IEEE RFID-TA Best Student Paper Award. He was the TPC Chair of the IEEE IMS 2008 Symposium and the Chair of the 2005 IEEE CEM-TD Workshop. He is the Vice Chair of the RF Technical Committee (TC16) of the IEEE CPMT Society. He is the Founder and the Chair of the RFID Technical Committee (TC24) of the IEEE MTT Society and the Secretary/Treasurer of the IEEE C-RFID. He is an Associate Editor of the IEEE TRANSACTIONS ON MICROWAVE THEORY AND TECHNIQUES, the IEEE TRANSACTIONS ON ADVANCED PACKAGING, and the *International Journal on Antennas and Propagation*. He has given over 100 invited talks to various universities and companies all over the world. He served as one of the IEEE MTT-S Distinguished Microwave Lecturers from 2010 to 2012. He is one of the IEEE CRFID Distinguished Lecturers.